iScience

CellPress
OPEN ACCESS

Article

Human Lung Adenocarcinoma-Derived Organoid Models for Drug Screening

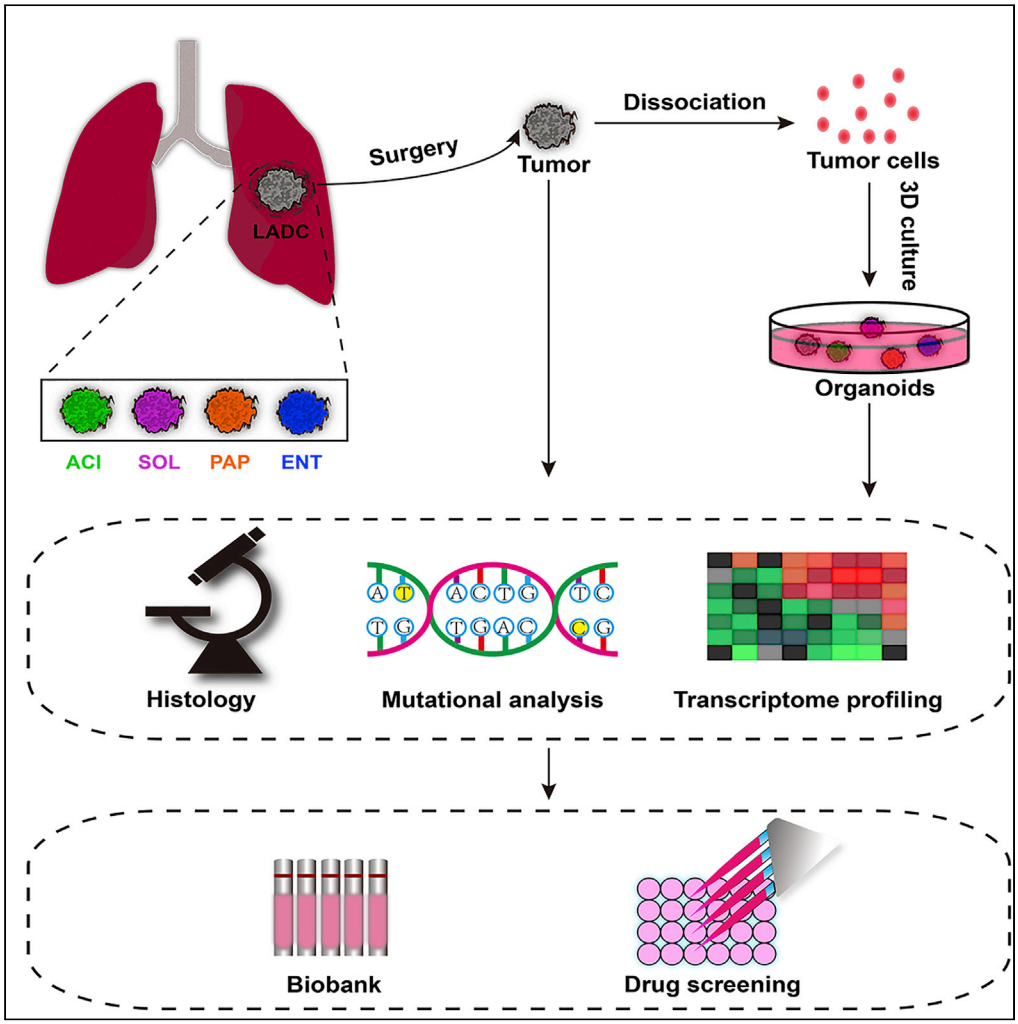

Zhichao Li, Youhui Qian, Wujiao Li, ..., Zhiming Cai, Wei Chen, Weiren Huang

jessie_chenwei@163.com (W.C.)
pony8980@163.com (W.H.)

HIGHLIGHTS

Generation of a living biobank of patient-derived lung adenocarcinoma organoids

Organoid biobank encompasses most of known subtypes of adenocarcinoma

Organoids maintain the histological and mutational spectrum of original tumors

Tumor organoids provide a tool for biomarker identification and drug testing

Li et al., iScience *23*, 101411
August 21, 2020
https://doi.org/10.1016/j.isci.2020.101411

iScience

CellPress
OPEN ACCESS

Article

Human Lung Adenocarcinoma-Derived Organoid Models for Drug Screening

Zhichao Li,[1,3,5,6] Youhui Qian,[1,6] Wujiao Li,[1,3,5,6] Lisa Liu,[1,3,5] Lei Yu,[1,3,5] Xia Liu,[1] Guodong Wu,[1] Youyu Wang,[1] Weibin Luo,[1] Fuyuan Fang,[1] Yuchen Liu,[1,3,5] Fei Song,[1,3,5] Zhiming Cai,[1,2,3,4,5] Wei Chen,[1,3,4,5,*] and Weiren Huang[1,2,3,4,5,6,7,*]

SUMMARY

Lung cancer is an extremely heterogeneous disease, and its treatment remains one of the most challenging tasks in medicine. Few existing laboratory lung cancer models can faithfully recapitulate the diversity of the disease and predict therapy response. Here, we establish 12 patient-derived organoids from the most common lung cancer subtype, lung adenocarcinoma (LADC). Extensive gene and histopathology profiling show that the tumor organoids retain the histological architectures, genomic landscapes, and gene expression profiles of their parental tumors. Patient-derived lung cancer organoids are amenable for biomarker identification and high-throughput drug screening *in vitro*. This study should enable the generation of patient-derived lung cancer organoid lines, which can be used to further the understanding of lung cancer pathophysiology and to assess drug response in personalized medicine.

INTRODUCTION

Lung cancer is the leading cause of cancer-related mortality globally. Every year, an estimated 1.82 million people are diagnosed with lung cancer and 1.56 million die from the disease (Ferlay et al., 2015). Lung cancer is divided into two main histological classes: non-small-cell lung cancer (NSCLC, ~85%) and small-cell lung cancer (SCLC, ~15%) (Herbst et al., 2008). There are two main histological subtypes of NSCLC: lung squamous-cell carcinoma (LSCC) and lung adenocarcinoma (LADC) (Molina et al., 2008). LADC has been the most predominant subtype of lung cancer since 1980s in the United States, and its incidence rates have been rising, whereas LSCC rates have been declining (Devesa et al., 2005; Patel et al., 2015).

Despite the considerable advances in the understanding of LADC, medical management is largely empirical and based on clinical and pathological features. However, owing to tumor heterogeneity among patients, clinical outcomes are usually unsatisfactory. The overall 5-year survival rate for lung cancer is 18% for all cancer stages combined in the United States (Siegel et al., 2018). Precision medicine, in which treatment regimens are individually tailored to each patient based on tumor characteristics, is believed to improve clinical outcomes. However, the development of precision medicine for LADC has been hampered by the lack of *in vitro* models in which the efficacy of candidate therapeutic regimens can be assessed.

The most commonly used LADC models are two-dimensional (2D) cell lines and patient-derived xenografts (PDXs). Although lung cancer cell lines, such as the LC2/ad cell line, PC-9 cell line, and VMRC-LCD cell line, have enabled advances in our understanding of lung cancer pathogenesis, they cannot fully recapitulate the three-dimensional (3D) structure of original tumors and do not retain the mutational profiles of their parental tumors (Suzuki et al., 2015). The PDX model retains the lung cancer mutational spectrum and the 3D organization, but the establishment of this model is inefficient and labor-intensive and usually takes several months per case, which makes it impractical to apply this model to guide precision medicine (Morgan et al., 2017; Moro et al., 2012). Therefore, there is an urgent necessity to establish a suitable model of LADC that faithfully recapitulates every aspect of its parental tumor and allows for large-scale drug screening.

Over the past few years, three-dimensional cancer organoid culture systems have been established from various cancers, including prostate cancer, colorectal cancer, pancreatic cancer, liver cancer, breast cancer,

[1]Shenzhen Second People's Hospital, The First Affiliated Hospital of Shenzhen University, Shenzhen, Guangdong 518035, China

[2]Shenzhen Institute of Synthetic Biology, Shenzhen Institutes of Advanced Technology, Chinese Academy of Sciences, Shenzhen, Guangdong 518055, China

[3]International Cancer Center, Shenzhen University School of Medicine, Shenzhen, Guangdong 518060, China

[4]The First Affiliated Hospital of Shantou University, Shantou, Guangdong 515041, China

[5]Guangdong Key Laboratory of Systems Biology and Synthetic Biology for Urogenital Tumors, Shenzhen, Guangdong 518035, China

[6]These authors contributed equally

[7]Lead Contact

*Correspondence: jessie_chenwei@163.com (W.C.), pony8980@163.com (W.H.)

https://doi.org/10.1016/j.isci.2020.101411

bladder cancer, and gastric cancer (Boj et al., 2015; Broutier et al., 2017; Gao et al., 2014; Lee et al., 2018; Sachs et al., 2018; van de Wetering et al., 2015; Yan et al., 2018). These cancer organoids have been shown to preserve the histological and mutational characteristics of their corresponding tumors and allow for drug screening. Several laboratories have established patient-derived lung cancer organoid lines from different histological and clinical stages as preclinical models for therapeutic drug screening (Kim et al., 2019; Li et al., 2020; Sachs et al., 2019; Shi et al., 2020).

In this study, we established 12 LADC organoid lines from tumor resections. In addition, we provided a thorough phenotypic and molecular characterization of LADC organoid lines and their parental tumors, including histological architecture, clinical marker expression, genomic landscape, and expression profile. Furthermore, we demonstrated the utility of LADC organoid lines as a model for drug testing to identify new therapeutic targets and advance personalized medicine. This study should be complementary to previous reports by providing a biobank of LADC organoids that covers a large spectrum of different LADC subtypes, including acinar (ACI), solid (SOL), papillary (PAP), and enteric (ENT) adenocarcinoma. We demonstrate that mechanical dissociation method is more suitable for the passage of LADC organoids. By comparing the transcriptome of LADC organoids with that of normal lung tissue-derived organoids, we identified several potential biomarkers associated with survival status when their expression levels were altered.

RESULTS

Establishment of a Living Biobank of Patient-Derived LADC Organoids

Surgically resected lung adenocarcinoma samples were obtained from untreated patients under informed consent. Each sample was split into four parts for organoid culture, histological analysis, genomic analysis, or transcriptomic analysis (Figure 1A). To isolate tumor cells, the resected tissue was minced with scissors and then digested with collagenase type II and trypsin. Tumor cells were plated in Matrigel drops and overlaid with organoid culture medium (Table S1). For the passaging of lung adenocarcinoma organoids, we first adopted the enzyme digestion protocol described in several reports (Li et al., 2018; Sachs et al., 2019). However, we noticed some lung adenocarcinoma organoid lines stopped growing after passaging (Figure S1). This problem was solved by using the mechanical dissociation method (see Transparent Methods). Organoid lines successfully maintained over five passages were regarded as success in organoid establishment. Using this protocol, we successfully established 12 human LADC-derived organoids from 15 patients with different subtypes of LADC (Table S2). The growth and passage of these LADC organoids were recorded (Figure 1B).

LADC Organoids Preserve the Histological Structure of Parental Tumors

The majority of lung adenocarcinoma are classified into acinar (ACI), solid (SOL), papillary (PAP), micropapillary (MIP), or lepidic (LEP) subtypes based on their predominant histologic pattern (Eguchi et al., 2014; Mengoli et al., 2018; Travis et al., 2013).To test whether LADC organoids maintain the histological patterns present in the original patient samples, we performed hematoxylin and eosin (H&E) staining of paraffin sections from the organoids, as well as their corresponding parental tumors. The histological features of the parental tumors were highly recapitulated in the LADC organoid lines. For example, the LADC organoids from ACI adenocarcinoma presented a glandular and cystic-like structure, whereas the LADC organoids derived from SOL adenocarcinoma showed a solid and compact pattern (Figures 1C and S2). One LADC organoid line, ENT-1_O, established from an enteric adenocarcinoma sample, displayed a histological morphology similar to metastatic colorectal carcinoma, as observed in its corresponding parental tissue (Figure 1C). Compared with the normal lung organoids, which displayed a well-organized structure, LADC organoids always showed typical cancerous characteristics, such as enlarged nuclei and mucinous glands (Figures 1C and S2).

To further characterize our LADC organoid lines, we performed immunofluorescence analysis of epithelial specific marker expression in each organoid line, as well as their corresponding parental tumors. We examined the expression of two adenocarcinoma markers, thyroid transcription factor (TTF-1) and Napsin A (Travis et al., 2010), as well as luminal epithelial marker cytokeratin 7 (CK7). All the organoid lines and their parental tumors were also stained for the most specific and sensitive squamous cell marker p40 (Tatsumori et al., 2014) and the basal epithelial marker cytokeratin 5 (CK5) to distinguish these LADC samples from LSCC samples. Most of the LADC organoid lines and the corresponding parental tumors exhibited positive staining of TTF-1 (n = 8/12) and Napsin A (n = 10/12), consistent with previous reports (Fatima et al., 2011;

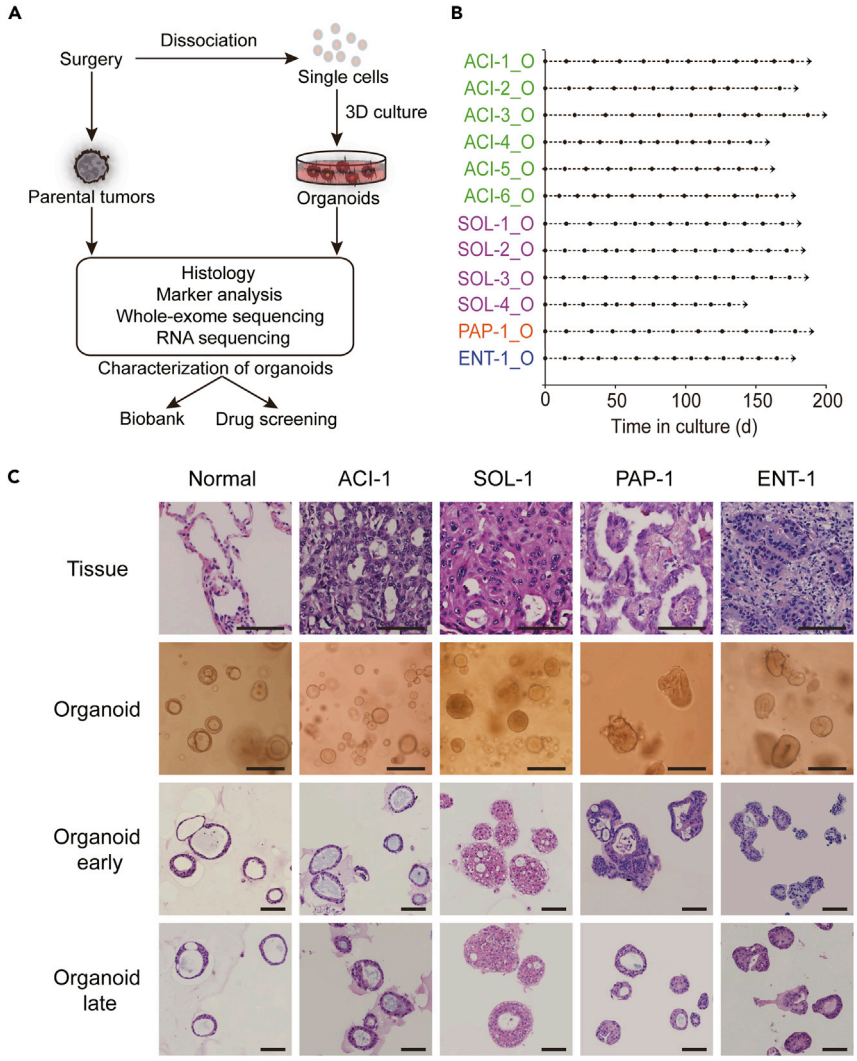

Figure 1. Establishment of Patient-Derived LADC Organoids

(A) Overview of experimental design.

(B) Expansion potential of LADC organoids established. Arrow, continuous expansion. Dot, passage.

(C) Representative H&E staining of LADC tissues together with the bright-field images and H&E staining of the organoids derived from corresponding tumor tissues. Early passage (passage 5–10) and late passage (>10). Scale bar, 100 μm.

See also Figure S2, Tables S1 and S2.

Gurda et al., 2015), and none of them were positive for CK5 and p40 (Figures 2 and S3). All the organoid lines displayed concordant marker expression profiles in the corresponding parental tumors. For example, TTF-1 was highly expressed in the ACI-1 and PAP-1 organoid lines and in their parental tissues but was absent in the SOL-1 and ENT-1 organoid lines and their parental tumors (Figure 2). Likewise, Napsin A was not expressed in the ENT-1 and ACI-3 organoid lines, in agreement with the expression pattern of their corresponding parental tumors, whereas the rest of the LADC organoid lines and their parental tumors were positive for Napsin A (Figures 2 and S3). All of the LADC organoid lines and their parental tumors expressed CK7, confirming an epithelial origin for all the organoids. Tumor samples and corresponding organoids also displayed a concordant expression pattern of Surfactant protein C (SFTPC), suggesting that alveolar type 2 (AT2) cells could be the cells of origin of these $SFTPC^{+}$ samples (Figure 2).

In summary, these results demonstrate that the histological architecture and marker expression of the parental LADC tissues were recapitulated in the LADC organoids, even after long-term culture *in vitro*.

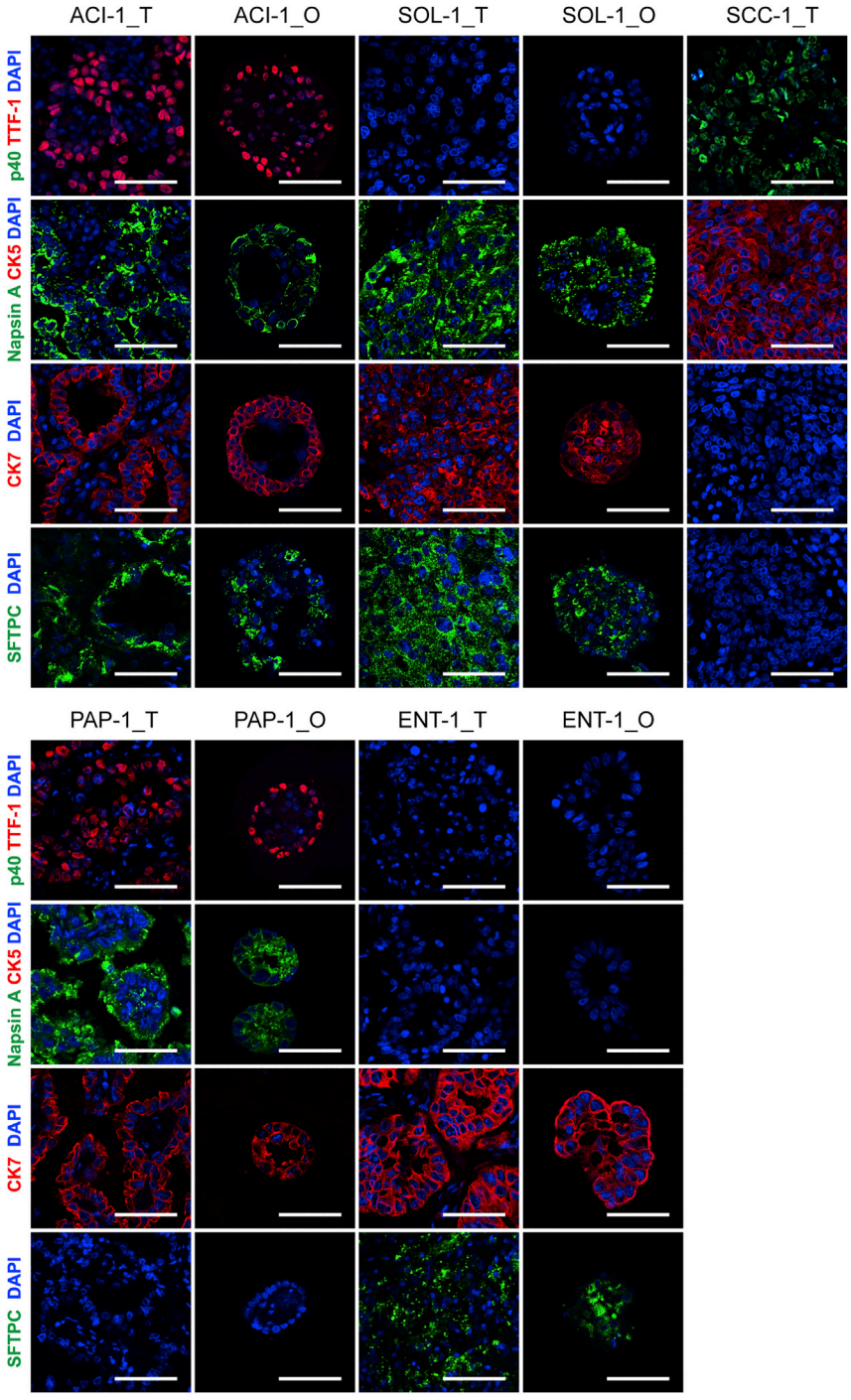

Figure 2. LADC-Derived Organoids Recapitulate Histopathological Characteristics of Parental Tumors

Representative immunofluorescence images of paired LADC organoids (_O) and tumor tissues (_T) for TTF-1, Napsin A, p40, CK5, CK7, and SFTPC. Nuclei were stained with DAPI (blue). One lung squamous cell carcinoma sample, SCC-1_T, was also stained for these markers as a control. Scale bar, 100 μm. See also Figure S3 and Table S3.

LADC Organoid Lines Retain the Mutational Spectrum of the Parental Tumors

To determine whether the LADC organoid lines retain the genetic mutations present in the parental tumors, we performed whole-exome sequencing (WES) of the organoid lines and compared the results with those of the corresponding parental tumors. We filtered for variants and excluded polymorphisms

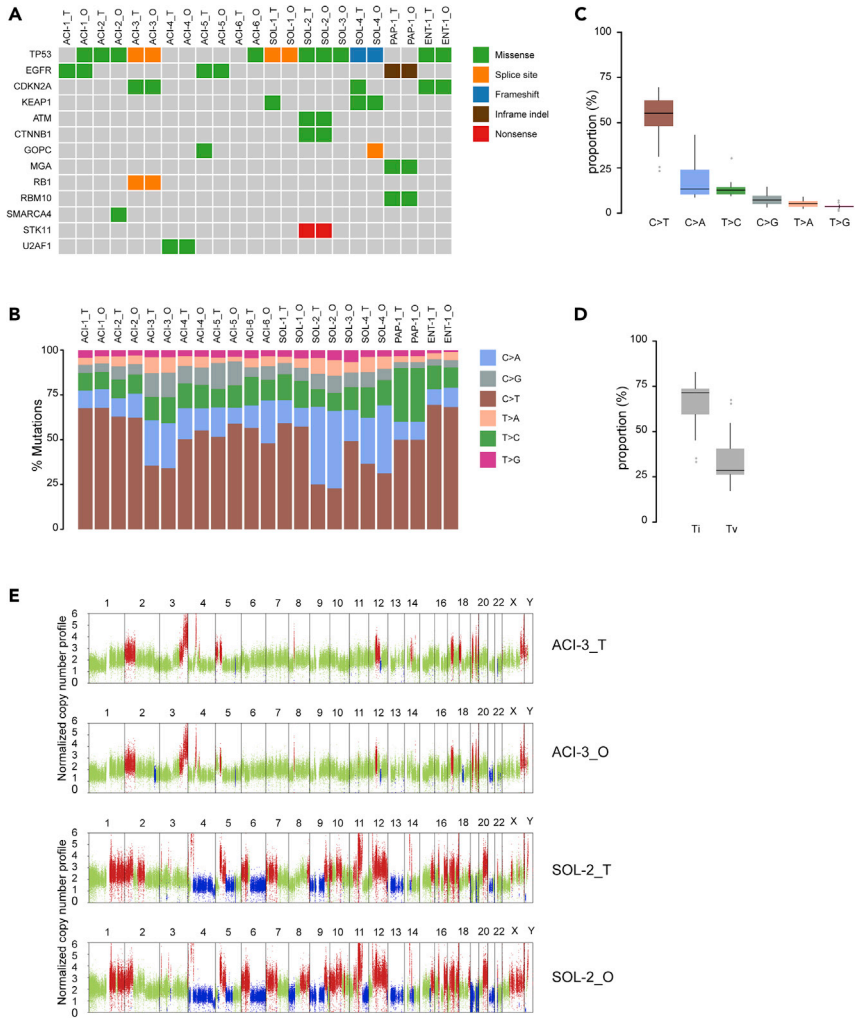

Figure 3. Mutational Signatures in LADC Organoid Lines

(A) Summary of somatic mutations detected by deep targeted sequencing of LADC organoids (_O) and parental tumors (_T) where available. The type of mutation is indicated in the legend.

(B) Proportions of exonic variants in LADC organoids (_O) and parental tumors (_T) and the six types of base substitutions are represented and indicated in the legend.

(C) Percentage of the six types of base substitutions across all samples. Graph shown are mean ± SD.

(D) Percentage of C>T/G>A transitions (Ti) and C>A/G>T transversions (Tv) across all samples. Graphs shown are mean ± SD.

(E) Representative copy number landscape of paired LADC organoids (_O) and tumor tissues (_T). Red and blue represent DNA copy number gains and losses.

See also Tables S4 and S5.

present in organoid lines and parental tumors by comparing them to the analysis of matched patients' normal blood. The 12 LADC organoid lines displayed a heterogeneous set of cancer driver genes affected by missense mutations, splice site mutations, or frameshift mutation, some of which showed a variable pattern of alteration (Figure 3A). Comparative analysis showed that the somatic mutations present in the parental tumor tissue were highly retained in the corresponding LADC organoid lines. Importantly, the LADC organoid lines retained the majority of the most common genetic mutations in human LADC (Cancer Genome Atlas Research Network, 2014; Imielinski et al., 2012; Jordan et al., 2017). For example, *TP53*, the most commonly mutated gene in LADC, was mutated in most LADC organoid lines and their corresponding tumors (Figure 3A). We also identified cancer-associated mutated genes, including *EGFR*, *CDKN2A*, *KEAP1*, *ATM*, *CTNNB1*, *GOPC*, *MGA*, and *RB1*, almost all of which were conserved between organoid lines

and parental tumors (Figure 3A; Table S4). We noticed that both the ACI-1_O and ACI-6_O lines harbored a *TP53* missense mutation, which is absent in their parental tumors (Figure 3A). This is likely to be explained by the pure tumor cellularity in the organoids or the intratumor diversification of the tumor samples.

To further determine the extent to which LADC organoid lines maintain the mutation spectrum of their parental tumors, we analyzed somatic substitutions in both tumor samples and organoids. The proportion of base substitutions was well retained among the LADC tissues and the corresponding cancer organoids (Figure 3B). Additionally, the most frequent base substitutions for both LADC tumor samples and organoids were C>T/G>A transitions (Ti) and C>A/G>T transversions (Tv), whereas the least frequent mutation type was T>G/A>C transversions (Figures 3B–3D), in agreement with the mutational spectrum described for LADC (Imielinski et al., 2012). Copy number variations (CNVs) analysis revealed similar patterns of DNA copy number gains and losses among LADC organoid lines and their corresponding tumors (Figure 3E; Table S5).

Intra-tumoral heterogeneity is a feature of LADC and may impact patient response to therapy. To assess whether intra-tumoral heterogeneity exists in LADC samples, we collected several parts of tumor tissues from one patient and sent them for whole-exome sequencing. Each tumor tissue was divided into three parts, and two tumor samples were collected. Genomic landscapes analysis revealed that subregion-specific genomic variants existed in different areas of the same tumor (Figure S4). For example, a *CCER1* missense mutation and a *CNTNAP3* missense mutation existed in the second part of sample ACI-7 but not in the other two subregions.

LADC Organoids Recapitulate the Transcriptome of the Corresponding Parental Tumors

To further characterize our organoid lines, we performed RNA sequencing (RNA-seq) on LADC organoid lines and the corresponding tumor tissues. We compared the RNA-seq data of the LADC organoids with 541 LADC expression datasets from The Cancer Genome Atlas (TCGA) to determine whether our organoids were representative of the overall population of LADC. The results show that our organoids were distributed randomly throughout the dataset, suggesting representative gene expression profiles (Figure 4A). Gene expression correlation analysis showed that each LADC organoid line displayed a high concordance of expression profile to its corresponding tumor but not to any of the other tumor samples (Figure 4B). One exception was the ACI-6 line, the expression profile of which failed to highly correlate with its corresponding tumor, by failing to keep the lost *TP53* mutation seen in the tumor. In addition to global gene expression, we also evaluated the gene expression overlap in LADC-specific upregulated genes. These genes were identified by comparing the transcriptomes of LADC tumor samples with normal lung tissues from TCGA (>2-fold change, $p < 0.05$). The top 50 upregulated genes were selected in this study. The results showed that LADC organoids largely maintained the expression signatures of LADC-specific genes (Figure S5).

LADC Organoids as a Model to Identify Potential Biom arkers

In addition to LADC organoids, we also established three normal lung organoid lines (N-1_O, N-2_O, N-3_O) from normal wild-type lung samples. To explore the potential of LADC organoids as a model to identify tumor biomarkers, we compared the transcriptomes of all LADC organoid lines to those of all normal lung organoid lines. First, we performed principal component analysis (PCA) to determine the contribution of the cancerous state to the difference in gene expression between LADC organoids and normal lung organoid lines. The resulting data showed that normal lung organoids clustered together, whereas the LADC organoids were scattered all around, showing the tumor heterogeneity among patients (Figure 5C). Most LADC organoids belong to the same subtypes clustered together, with the exception of SOL-4_O line clustering with PAP-1_O and ACI-2_O clustering with ENT-1_O. PC1 component accounted for the variance between LADC organoids and normal lung organoids.

Next, we searched for differentially expressed genes between LADC organoids and normal lung organoids. Thirty upregulated genes and 30 downregulated genes with the lowest p values were selected for our analysis; we found that 20 genes had been reported to be upregulated and 11 genes had been reported to be downregulated in LADC, including *CA9*, *NT5E*, *EFCC1*, and *SERPINE1* (Figure 5A). We then studied the prognostic values of the remaining genes by performing survival analysis using publicly available TCGA databases. Within the 29 novel genes whose expression levels have never been reported to be altered in LADC samples, four genes were shown to be associated with survival status when their expression levels were altered (Figure 5B). *RHOF*, *SLC16A3*, and *ANXA10* predicted poor prognosis when overexpressed,

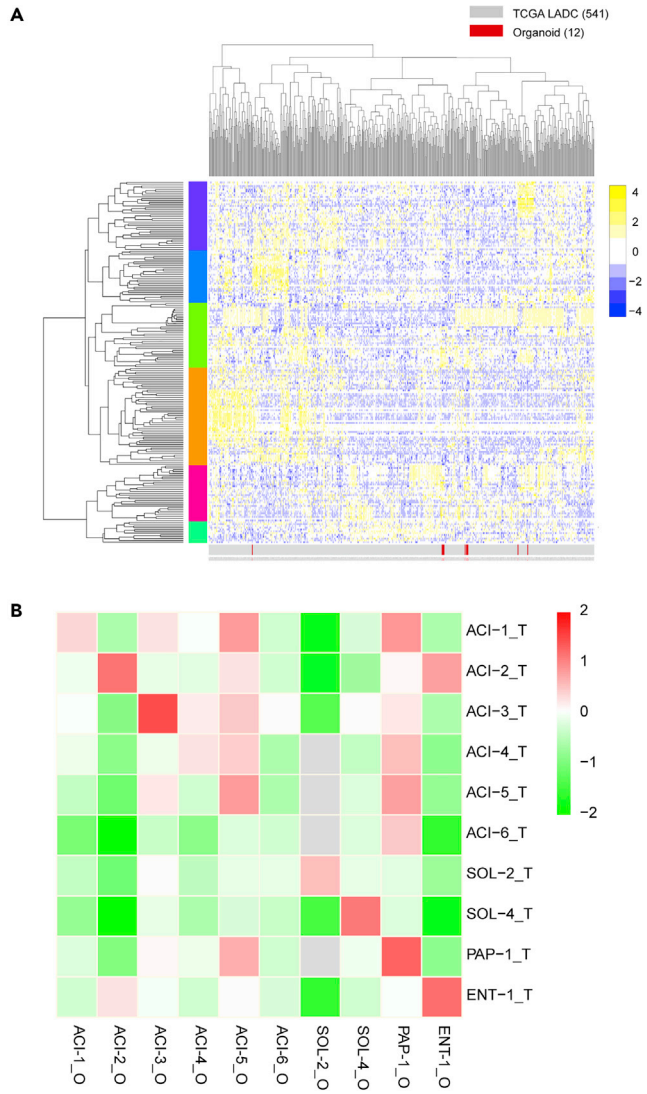

Figure 4. Global Gene Expression Analysis of LADC Organoids

(A) RNA-seq data of 12 LADC organoid lines were normalized and combined with TCGA RNA-seq data (541 samples). The combined data were clustered using the 500 most-variable genes using 1-correlation distance with complete linkage.

(B) Correlation heatmap of LADC organoids (_O) and tumor tissues (_T) based on RNA-seq expression data. Correlations were calculated for all paired organoids and tumors using all genes (column z-scored).

See also Figure S5.

whereas the downexpression of *CDHR1* correlated with poor overall survival (Figure 5B). Of one note was that *HOXB6* was also found to be upregulated in our LADC organoids and high expression was also associated with poor survival in patients with LADC. These data suggest that LADC organoids could be used as a model to identify tumor biomarkers.

We also performed KEGG (Kyoto Encyclopedia of Genes and Genomes) analysis to search for signaling pathways altered in LADC organoids. We found that the most enriched pathways in LADC organoids were the PI3K-Akt signaling pathway, pathways related to focal adhesion, complement and coagulation cascades, and the ECM-receptor interaction-associated pathways (Figure 5D).

LADC Organoid Lines as a Model for Drug Screening

In order to evaluate the utility of lung adenocarcinoma organoids as a platform to predict patient-specific sensitivities to anticancer drugs, we performed high-throughput drug dose-response screens in 12 lung

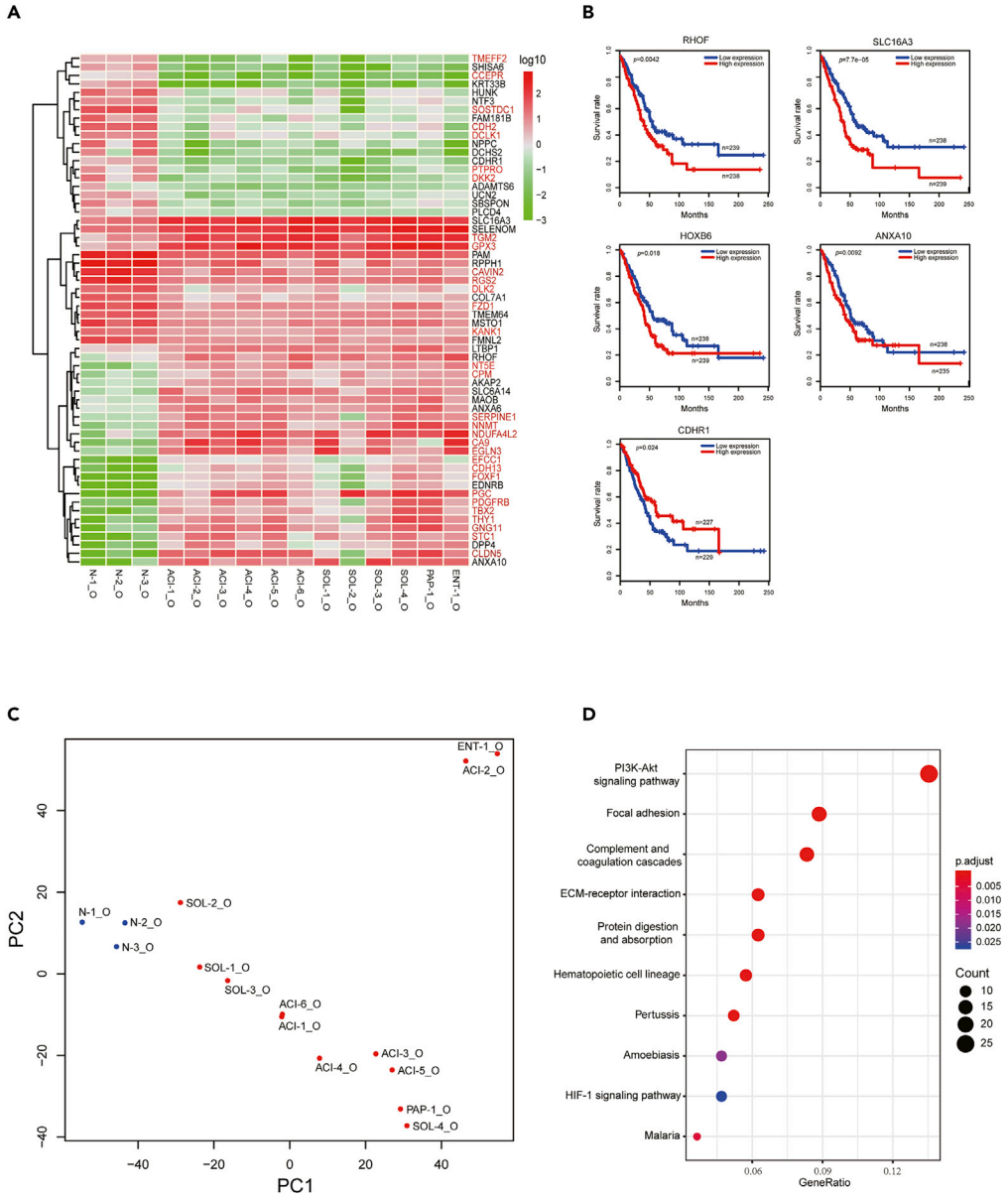

Figure 5. Use of LADC Organoids to Identify Tumor Biomarkers

(A) Heatmap of 60 differentially expressed genes in LADC organoids, compared with normal lung organoids. Red indicates high expression; green indicates low expression. Genes marked in red were reported by others.

(B) Kaplan-Meier survival analysis of patients with LADC based on the expression level of the indicated genes.

(C) Principal components analysis (PCA) of RNA-seq data of all LADC organoids and normal lung organoids.

(D) Significantly enriched KEGG signaling pathways in LADC organoids, compared with normal lung organoids.

adenocarcinoma organoid lines. LADC organoid cultures were gently collected and plated in low-attachment 96-well plates in 2% Matrigel/growth medium. Organoids were treated with drugs 1 day after plating and incubated for 6 days before measuring the cell number using Cell Titer-Glo 3D reagent. For each lung adenocarcinoma organoid line, we tested its sensitivity to a library of 24 anti-cancer drugs using dose titration assays with technical replicates and biological triplicates (different passages of the same organoid line, between passages 5 and 10). Drugs were selected based on their clinical relevance for lung cancer treatment, including standard chemotherapy drugs and targeted agents against signaling pathways or molecules of interest. Drug sensitivity is shown by the half-maximal inhibitory concentration (IC_{50}) and by the area under the dose-response curve (AUC).

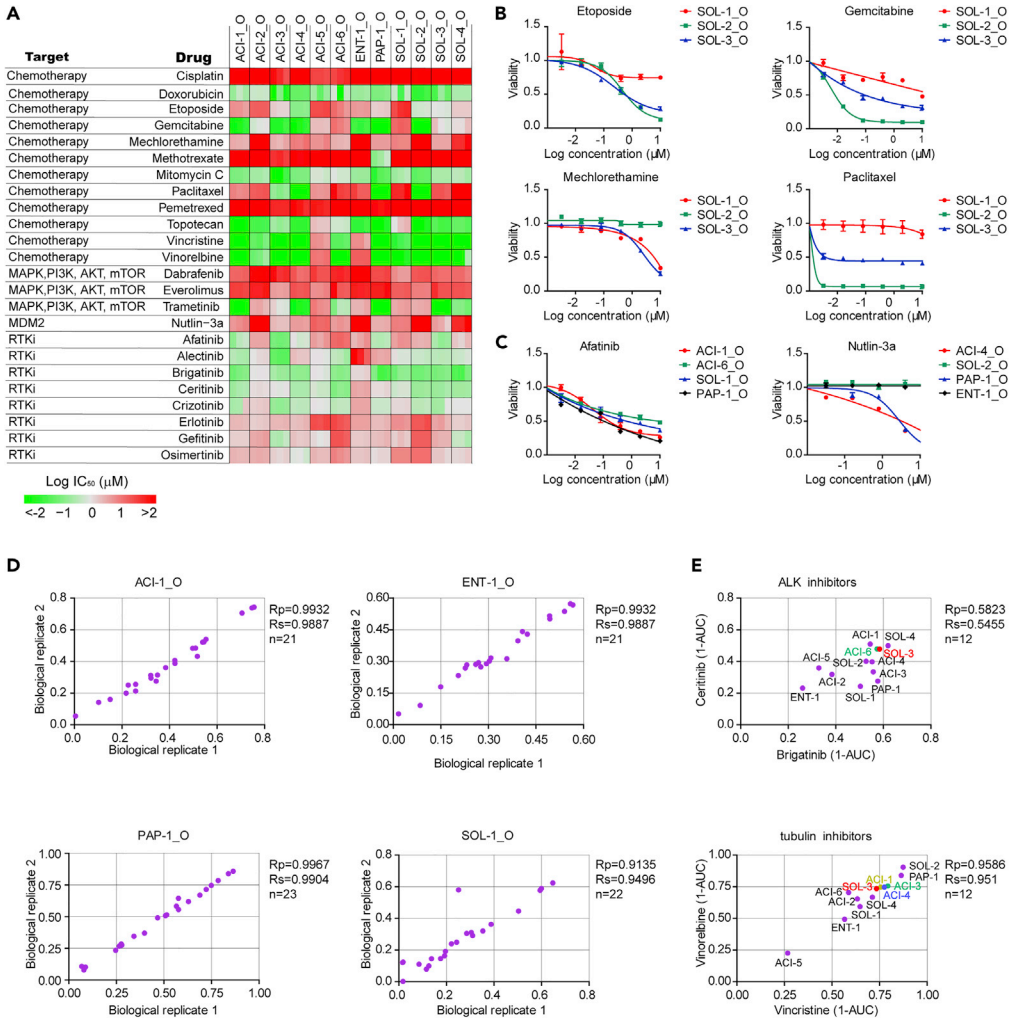

Figure 6. High-Throughput Drug Screening in LADC Organoids

(A) Heatmap of logIC_{50} values for 24 compounds against LADC organoids by applying nonlinear regression (curve fit).

(B and C) Dose-response curves of organoid lines to selected drugs. Each data point represents three biological replicates, with error bars representing ±SEM.

(D) Representative scatterplots of 1-AUC (area under the curve) from two biological replicates of the drug screening data. Each data point is the 1-AUC for a drug used to treat the organoid line.

(E) Representative scatterplots of 1-AUC from drug screening data of paired drugs with the same nominal targets..

See also Figure S6 and Table S6.

For each organoid line, its sensitivity to each particular drug was consistent between different passages, as revealed by the IC_{50} results and the high positive correlation of AUC values across biological replicates (Figures 6A and 6D). Individual lung adenocarcinoma organoid lines varied greatly in their responses to drugs owing to tumor heterogeneity. For example, the SOL-2_O organoid line was highly sensitive to gemcitabine, paclitaxel, and etoposide and resistant to mechlorethamine, whereas SOL-1_O line was sensitive to mechlorethamine and resistant to gemcitabine, paclitaxel, and etoposide (Figures 6A and 6B). Of particular interest was the PAP-1_O line with methotrexate, in which case we observed much higher sensitivity than that in all the rest of the LADC organoid lines (Figure 6A).

We also observed that drugs with similar nominal targets had comparable activity across all the LADC organoid lines. For example, the tubulin inhibitors vincristine and vinorelbine displayed similar sensitivity patterns and all the organoid lines showed a similar and concordant trend for the ALK-targeted drugs brigatinib and ceritinib (Figures 6A and 6E).

Some of the differences in responses to drugs between LADC organoid lines were in correlation with their mutational profiles. For example, the SOL-2_O line and ENT-1_O line displayed resistance to the p53-stablizing drug nutlin-3a, consistent with the presence of inactivating mutations in *TP53* (Vassilev et al., 2004) (Figure 6C). All the three organoid lines ACI-4_O, ACI-6_O, and PAP-1_O that were wild-type for *TP53* were sensitive to nutlin-3a (Figure S6). The organoid lines ACI-1_O and PAP-1_O demonstrated responses to the EGFR targeting agent afatinib, consistent with *EGFR* mutations in both samples (Figures 6A and 6C). Of note, the organoid lines ACI-3_O and SOL-3_O also demonstrated sensitivity to afatinib despite not having mutations in *EGFR* (Figure 6A), emphasizing the value of WES in combination with *in vitro* drug screens on LADC organoids.

We also observed a number of drugs with differential activities in the absence of an apparent genetic biomarker. For example, half of the LADC organoid lines were relatively more sensitive to trametinib, a MEK inhibitor, than the other half of the samples (Figure 6A). The ACI-3_O line and SOL-4_O line were sensitive to gefitinib, even though they did not harbor *EGFR* mutations (Figure 6A), highlighting the value of functional drug tests on LADC organoids.

DISCUSSION

In this study, we demonstrate the feasibility of generating cancer organoid lines from clinical LADC samples. A living biobank of 12 LADC organoid lines was generated from the most common LADC subtypes with a success rate of 80% (12/15). Compared with the conventional enzymatic digestion method, we demonstrate that the mechanical dissociation method in which the organoids are smashed into small fragments using 10-mL Stripette Serological Pipets is a better option for the passage of LADC organoids.

Comprehensive characterization of the LADC organoid lines confirm that they recapitulate the features of the corresponding parental tumors in terms of histological architecture, cancer driver gene mutations, copy number alterations (CNVs), single-nucleotide variants (SNV), and global gene expression profiles, even after long-term culture *in vitro*.

As LADC organoids preserve the genomic characteristics and global genes expression profiles of their corresponding parental tumors, we used LADC organoids as a model to identify tumor biomarkers. We found that the expression of *RHOF*, *SLC16A3*, *HOXB6*, *ANXA10*, and *CDHR1*, which was not reported to be altered in clinical LADC samples, was associated with survival status of patients with LADC and could be used as prognostic factors. The advantage of using LADC organoids over clinical LADC samples to search for tumor biomarkers is that LADC organoids are purer, so the differences in gene expression between tumor cells and nontumor cells are not affected by the presence of stromal cells and immune cells. Furthermore, the mechanism by which these tumor biomarkers affect tumor behaviors could be studied at the organoid level when combined with molecular biology techniques.

Lung cancer is generally thought to originate from the malignant transformation of adult lung stem cells (Wang et al., 2020; Zhang et al., 2015). LADC is believed to originate from alveolar type 2 (AT2) cells or their progenitors. *KRAS* (G12D) mutation in AT2 cells generates multifocal, clonal adenomas in transgenic mice (Desai et al., 2014). Another study demonstrates that $CC10^{+}$ AT2 cells can give rise to LADC in response to *KRAS* (G12D) activation in mice (Xu et al., 2012). A recent study proves that the $Sca\text{-}1^{+}Abcg1^{+}$ bronchioalveolar epithelial cells are the cancer stem cell-like subset of AT2 cells and are the origin of LADC in *GPRC5A*-knockout mice (Yin et al., 2020). In addition to AT2 cells, Club cells are also shown to survive *KRAS* mutations and to form LADC after tobacco carcinogen exposure (Spella et al., 2019). Bronchoalveolar stem cells (BASCs) can proliferate *in vitro* and are expanded at early stages of tumorigenesis *in vivo* following *KRAS* (G12D) mutation, suggesting that BASCs may be the cell of origin for LADC (Kim et al., 2005).

Stage IV NSCLC accounts for approximately 40% of newly diagnosed lung cancer cases (Lemjabbar-Alaoui et al., 2015; Zappa and Mousa, 2016). Chemotherapy is one of the most common treatments for stage IV NSCLC. However, there are no reliable biomarkers for predicting its efficacy, which may be influenced by histology, age, and performance status. Targeted therapy, which works by specifically targeting molecular abnormalities present in the tumor cells, has proved to increase survival rate in patients with lung cancer (Camidge et al., 2012; Ou et al., 2016; Yang et al., 2015). Although the target gene mutations can be detected by WES, the patients' responses to targeted therapies were not always consistent with the

expectations (Hirsch et al., 2017; Janne et al., 2015; Shaw et al., 2013). Thus, there is an urgent need to establish a suitable model to predict the patients' responses to chemotherapy and targeted therapy to increase the success rate.

Although suitable for high-throughput drug testing, traditional lung adenocarcinoma cell lines lack tissue architecture and cellular heterogeneity and are rarely of clinical relevance for individual patients. Patient-derived xenografts models of lung adenocarcinoma retain tumor histopathology and global gene expression of the patient's tumor but are resource intensive, time-consuming, and unsuitable for high-throughput drug screening. LADC organoid lines provide an opportunity to bridge the gap between traditional lung adenocarcinoma cell lines and patient-derived xenograft animal models. The LADC organoids-based high-throughput drug testing, in combination with the characterization of mutational profiles, could generate a link between lung LADC, genetics, and clinical trials to make personalized therapy designs and elucidate druggable targets.

Previous studies reported the use of lung cancer organoids to test drug responses (Kim et al., 2019; Sachs et al., 2019; Shi et al., 2020). In our study, LADC organoids were subjected to a larger library of anticancer drugs, including chemotherapeutic drugs and targeted drugs. We demonstrate that high-throughput drug screening is feasible in our LADC organoid biobank. Drug screening assays revealed striking differences in responses to a library of compounds between LADC organoid lines. There was a positive correlation of IC_{50} data and AUC value across biological replicates. The drugs with the same targets displayed reproducible sensitivity patterns among LADC organoid lines. We also observed a correlation between some drug sensitivities and mutational profiles.

Previous studies suggest that patient-derived gastrointestinal and gastric organoids could recapitulate patients' drug responses in the clinic (Vlachogiannis et al., 2018; Yan et al., 2018). As a next step, we will perform coclinical trials to determine whether the response of patient-derived LADC organoids to drugs *in vitro* recapitulates patients' responses to the same drugs *in vivo*.

Limitations of the Study

High-throughput drug screening on organoids can facilitate personalized medicine and, when combined with WES and RNA-seq analysis, can contribute to the development of algorithms that accurately predict drug sensitivity. In this paper, this was hampered by the small sample size of patients. Collecting a larger number of LADC organoids would increase the statistical power to detect molecular markers of drug response.

Resource Availability

Lead Contact

Correspondence and requests for materials and reagents should be directed to and will be fulfilled by the Lead Contact, Weiren Huang (pony8980@163.com).

Materials Availability

All organoid lines generated in this study will be available from the Lead Contact.

Data and Code Availability

The WES and transcriptome data generated during this study are available at Sequence Read Archive (SRA):SRR12059123-SRR12059164, SRR12072311-SRR12072333.

METHODS

All methods can be found in the accompanying Transparent Methods supplemental file.

SUPPLEMENTAL INFORMATION

Supplemental Information can be found online at https://doi.org/10.1016/j.isci.2020.101411.

ACKNOWLEDGMENTS

This work was supported by the National Key R&D Program of China (2019YFA0906000), National Natural Science Foundation of China (81772737, 81772736, 81972867), National Science Foundation Projects of

Guangdong Province, China(2017B030301015, 2020A1515010235), the Shenzhen Municipal Government of China (JCYJ20170413161749433), the Sanming Project of Shenzhen Health and Family Planning Commission (SZSM201412018, SZSM201512037), and the China Postdoctoral Science Foundation Grant (2019M653215).

AUTHOR CONTRIBUTIONS

Conceptualization, Z.L., W.C., and W.H.; Methodology, Z.L. and Y.Q.; Software, W.L.; Formal Analysis, W.L.; Investigation, Z.L., L.L., L.Y., X.L., Y.W., W.L., F.F., Y.L., F.S., and Z.C.; Writing - Original Draft, Z.L.; Writing - Review & Editing, W.C. and W.H.; Resources, Y.Q. and W.H.; Supervision, W.C. and W.H.; Funding Acquisition, W.H., W.C., and Z.L.

DECLARATION OF INTERESTS

The authors declare that none of them have any conflict of interest.

Received: February 14, 2020
Revised: June 29, 2020
Accepted: July 23, 2020
Published: August 21, 2020

REFERENCES

Boj, S.F., Hwang, C.I., Baker, L.A., Chio, , II, Engle, D.D., Corbo, V., Jager, M., Ponz-Sarvise, M., Tiriac, H., Spector, M.S., et al. (2015). Organoid models of human and mouse ductal pancreatic cancer. Cell *160*, 324–338.

Broutier, L., Mastrogiovanni, G., Verstegen, M.M., Francies, H.E., Gavarro, L.M., Bradshaw, C.R., Allen, G.E., Arnes-Benito, R., Sidorova, O., Gaspersz, M.P., et al. (2017). Human primary liver cancer-derived organoid cultures for disease modeling and drug screening. Nat. Med. *23*, 1424–1435.

Camidge, D.R., Bang, Y.J., Kwak, E.L., Iafrate, A.J., Varella-Garcia, M., Fox, S.B., Riely, G.J., Solomon, B., Ou, S.H., Kim, D.W., et al. (2012). Activity and safety of crizotinib in patients with ALK-positive non-small-cell lung cancer: updated results from a phase 1 study. Lancet Oncol. *13*, 1011–1019.

Cancer Genome Atlas Research Network (2014). Comprehensive molecular profiling of lung adenocarcinoma. Nature *511*, 543–550.

Desai, T.J., Brownfield, D.G., and Krasnow, M.A. (2014). Alveolar progenitor and stem cells in lung development, renewal and cancer. Nature *507*, 190–194.

Devesa, S.S., Bray, F., Vizcaino, A.P., and Parkin, D.M. (2005). International lung cancer trends by histologic type: male:female differences diminishing and adenocarcinoma rates rising. Int. J. Cancer *117*, 294–299.

Eguchi, T., Kadota, K., Park, B.J., Travis, W.D., Jones, D.R., and Adusumilli, P.S. (2014). The new IASLC-ATS-ERS lung adenocarcinoma classification: what the surgeon should know. Semin. Thorac. Cardiovasc. Surg. *26*, 210–222.

Fatima, N., Cohen, C., Lawson, D., and Siddiqui, M.T. (2011). TTF-1 and Napsin A double stain: a useful marker for diagnosing lung adenocarcinoma on fine-needle aspiration cell blocks. Cancer Cytopathol. *119*, 127–133.

Ferlay, J., Soerjomataram, I., Dikshit, R., Eser, S., Mathers, C., Rebelo, M., Parkin, D.M., Forman, D., and Bray, F. (2015). Cancer incidence and mortality worldwide: sources, methods and major patterns in GLOBOCAN 2012. Int. J. Cancer *136*, E359–E386.

Gao, D., Vela, I., Sboner, A., Iaquinta, P.J., Karthaus, W.R., Gopalan, A., Dowling, C., Wanjala, J.N., Undvall, E.A., Arora, V.K., et al. (2014). Organoid cultures derived from patients with advanced prostate cancer. Cell *159*, 176–187.

Gurda, G.T., Zhang, L., Wang, Y., Chen, L., Geddes, S., Cho, W.C., Askin, F., Gabrielson, E., and Li, Q.K. (2015). Utility of five commonly used immunohistochemical markers TTF-1, Napsin A, CK7, CK5/6 and P63 in primary and metastatic adenocarcinoma and squamous cell carcinoma of the lung: a retrospective study of 246 fine needle aspiration cases. Clin. Transl. Med. *4*, 16.

Herbst, R.S., Heymach, J.V., and Lippman, S.M. (2008). Lung cancer. N. Engl. J. Med. *359*, 1367–1380.

Hirsch, F.R., Scagliotti, G.V., Mulshine, J.L., Kwon, R., Curran, W.J., Jr., Wu, Y.L., and Paz-Ares, L. (2017). Lung cancer: current therapies and new targeted treatments. Lancet *389*, 299–311.

Imielinski, M., Berger, Alice H., Hammerman, Peter S., Hernandez, B., Pugh, Trevor J., Hodis, E., Cho, J., Suh, J., Capelletti, M., Sivachenko, A., et al. (2012). Mapping the hallmarks of lung adenocarcinoma with massively parallel sequencing. Cell *150*, 1107–1120.

Janne, P.A., Yang, J.C., Kim, D.W., Planchard, D., Ohe, Y., Ramalingam, S.S., Ahn, M.J., Kim, S.W., Su, W.C., Horn, L., et al. (2015). AZD9291 in EGFR inhibitor-resistant non-small-cell lung cancer. N. Engl. J. Med. *372*, 1689–1699.

Jordan, E.J., Kim, H.R., Arcila, M.E., Barron, D., Chakravarty, D., Gao, J., Chang, M.T., Ni, A., Kundra, R., Jonsson, P., et al. (2017). Prospective comprehensive molecular characterization of lung adenocarcinomas for efficient patient matching to approved and emerging therapies. Cancer Discov. *7*, 596–609.

Kim, C.F., Jackson, E.L., Woolfenden, A.E., Lawrence, S., Babar, I., Vogel, S., Crowley, D., Bronson, R.T., and Jacks, T. (2005). Identification of bronchioalveolar stem cells in normal lung and lung cancer. Cell *121*, 823–835.

Kim, M., Mun, H., Sung, C.O., Cho, E.J., Jeon, H.J., Chun, S.M., Jung, D.J., Shin, T.H., Jeong, G.S., Kim, D.K., et al. (2019). Patient-derived lung cancer organoids as in vitro cancer models for therapeutic screening. Nat. Commun. *10*, 3991.

Lee, S.H., Hu, W., Matulay, J.T., Silva, M.V., Owczarek, T.B., Kim, K., Chua, C.W., Barlow, L.J., Kandoth, C., Williams, A.B., et al. (2018). Tumor evolution and drug response in patient-derived organoid models of bladder cancer. Cell *173*, 515–528.e517.

Lemjabbar-Alaoui, H., Hassan, O.U., Yang, Y.W., and Buchanan, P. (2015). Lung cancer: biology and treatment options. Biochim. Biophys. Acta *1856*, 189–210.

Li, X., Francies, H.E., Secrier, M., Perner, J., Miremadi, A., Galeano-Dalmau, N., Barendt, W.J., Letchford, L., Leyden, G.M., Goffin, E.K., et al. (2018). Organoid cultures recapitulate esophageal adenocarcinoma heterogeneity providing a model for clonality studies and precision therapeutics. Nat. Commun. *9*, 2983.

Li, Y.F., Gao, Y., Liang, B.W., Cao, X.Q., Sun, Z.J., Yu, J.H., Liu, Z.D., and Han, Y. (2020). Patient-derived organoids of non-small cells lung cancer and their application for drug screening. Neoplasma *67*, 430–437.

Mengoli, M.C., Longo, F.R., Fraggetta, F., Cavazza, A., Dubini, A., Ali, G., Guddo, F., Gilioli, E., Bogina, G., Nannini, N., et al. (2018). The 2015 World Health Organization classification of lung tumors: new entities since the 2004 classification. Pathologica *110*, 39–67.

Molina, J.R., Yang, P., Cassivi, S.D., Schild, S.E., and Adjei, A.A. (2008). Non-small cell lung cancer: epidemiology, risk factors, treatment, and survivorship. Mayo Clinic Proc. *83*, 584–594.

Morgan, K.M., Riedlinger, G.M., Rosenfeld, J., Ganesan, S., and Pine, S.R. (2017). Patient-derived xenograft models of non-small cell lung cancer and their potential utility in personalized medicine. Front. Oncol. *7*, 2.

Moro, M., Bertolini, G., Tortoreto, M., Pastorino, U., Sozzi, G., and Roz, L. (2012). Patient-derived xenografts of non small cell lung cancer: resurgence of an old model for investigation of modern concepts of tailored therapy and cancer stem cells. J. Biomed. Biotechnol. *2012*, 568567.

Ou, S.H., Ahn, J.S., De Petris, L., Govindan, R., Yang, J.C., Hughes, B., Lena, H., Moro-Sibilot, D., Bearz, A., Ramirez, S.V., et al. (2016). Alectinib in crizotinib-refractory ALK-rearranged non-small-cell lung cancer: a phase II global study. J. Clin. Oncol. *34*, 661–668.

Patel, M.I., Cheng, I., and Gomez, S.L. (2015). US lung cancer trends by histologic type. Cancer *121*, 1150–1152.

Sachs, N., de Ligt, J., Kopper, O., Gogola, E., Bounova, G., Weeber, F., Balgobind, A.V., Wind, K., Gracanin, A., Begthel, H., et al. (2018). A living biobank of breast cancer organoids captures disease heterogeneity. Cell *172*, 373–386.e310.

Sachs, N., Papaspyropoulos, A., Zomer-van Ommen, D.D., Heo, I., Böttinger, L., Klay, D., Weeber, F., Huelsz-Prince, G., Iakobachvili, N., Amatngalim, G.D., et al. (2019b). Long-term expanding human airway organoids for disease modeling. EMBO J. *38*, e100300.

Shaw, A.T., Kim, D.W., Nakagawa, K., Seto, T., Crino, L., Ahn, M.J., De Pas, T., Besse, B., Solomon, B.J., Blackhall, F., et al. (2013). Crizotinib versus chemotherapy in advanced ALK-positive lung cancer. N. Engl. J. Med. *368*, 2385–2394.

Shi, R., Radulovich, N., Ng, C., Liu, N., Notsuda, H., Cabanero, M., Martins-Filho, S.N., Raghavan, V., Li, Q., Mer, A.S., et al. (2020). Organoid cultures as preclinical models of non-small cell lung cancer. Clin. Cancer Res. *26*, 1162–1174.

Siegel, R.L., Miller, K.D., and Jemal, A. (2018). Cancer statistics, 2018. CA A Cancer J. Clin. *68*, 7–30.

Spella, M., Lilis, I., Pepe, M.A., Chen, Y., Armaka, M., Lamort, A.S., Zazara, D.E., Roumelioti, F., Vreka, M., Kanellakis, N.I., et al. (2019). Club cells form lung adenocarcinomas and maintain the alveoli of adult mice. eLife *8*, e45571.

Suzuki, A., Matsushima, K., Makinoshima, H., Sugano, S., Kohno, T., Tsuchihara, K., and Suzuki, Y. (2015). Single-cell analysis of lung adenocarcinoma cell lines reveals diverse expression patterns of individual cells invoked by a molecular target drug treatment. Genome Biol. *16*, 66.

Tatsumori, T., Tsuta, K., Masai, K., Kinno, T., Taniyama, T., Yoshida, A., Suzuki, K., and Tsuda, H. (2014). p40 is the best marker for diagnosing pulmonary squamous cell carcinoma: comparison with p63, cytokeratin 5/6, desmocollin-3, and sox2. Appl. Immunohistochem. Mol. Morphol. *22*, 377–382.

Travis, W.D., Rekhtman, N., Riley, G.J., Geisinger, K.R., Asamura, H., Brambilla, E., Garg, K., Hirsch, F.R., Noguchi, M., Powell, C.A., et al. (2010). Pathologic diagnosis of advanced lung cancer based on small biopsies and cytology: a paradigm shift. J. Thorac. Oncol. *5*, 411–414.

Travis, W.D., Brambilla, E., and Riely, G.J. (2013). New pathologic classification of lung cancer: relevance for clinical practice and clinical trials. J. Clin. Oncol. *31*, 992–1001.

Vassilev, L.T., Vu, B.T., Graves, B., Carvajal, D., Podlaski, F., Filipovic, Z., Kong, N., Kammlott, U., Lukacs, C., Klein, C., et al. (2004). In vivo activation of the P53 pathway by small-molecule antagonists of MDM2. Science *303*, 844–848.

Vlachogiannis, G., Hedayat, S., Vatsiou, A., Jamin, Y., Fernandez-Mateos, J., Khan, K., Lampis, A., Eason, K., Huntingford, I., Burke, R., et al. (2018). Patient-derived organoids model treatment response of metastatic gastrointestinal cancers. Science *359*, 920–926.

Wang, J., Li, X., and Chen, H. (2020). Organoid models in lung regeneration and cancer. Cancer Lett. *475*, 129–135.

van de Wetering, M., Francies, H.E., Francis, J.M., Bounova, G., Iorio, F., Pronk, A., van Houdt, W., van Gorp, J., Taylor-Weiner, A., Kester, L., et al. (2015). Prospective derivation of a living organoid biobank of colorectal cancer patients. Cell *161*, 933–945.

Xu, X., Rock, J.R., Lu, Y., Futtner, C., Schwab, B., Guinney, J., Hogan, B.L., and Onaitis, M.W. (2012). Evidence for type II cells as cells of origin of K-Ras-induced distal lung adenocarcinoma. Proc. Natl. Acad. Sci. U S A *109*, 4910–4915.

Yan, H.H.N., Siu, H.C., Law, S., Ho, S.L., Yue, S.S.K., Tsui, W.Y., Chan, D., Chan, A.S., Ma, S., Lam, K.O., et al. (2018). A comprehensive human gastric cancer organoid biobank captures tumor subtype heterogeneity and enables therapeutic screening. Cell Stem Cell *23*, 882–897.e11.

Yang, J.C., Sequist, L.V., Geater, S.L., Tsai, C.M., Mok, T.S., Schuler, M., Yamamoto, N., Yu, C.J., Ou, S.H., Zhou, C., et al. (2015). Clinical activity of afatinib in patients with advanced non-small-cell lung cancer harbouring uncommon EGFR mutations: a combined post-hoc analysis of LUX-Lung 2, LUX-Lung 3, and LUX-Lung 6. Lancet Oncol. *16*, 830–838.

Yin, H., Jiang, Z., Feng, X., Ji, Z., and Jin, W. (2020). Identification of Sca-1(+)Abcg1(+) bronchioalveolar epithelial cells as the origin of lung adenocarcinoma in Gprc5a-knockout mouse model through the interaction between lung progenitor AT2 and Lgr5 cells. Oncogene *39*, 3754–3773.

Zappa, C., and Mousa, S.A. (2016). Non-small cell lung cancer: current treatment and future advances. Transl. Lung Cancer Res. *5*, 288–300.

Zhang, D.G., Jiang, A.G., Lu, H.Y., Zhang, L.X., and Gao, X.Y. (2015). Isolation, cultivation and identification of human lung adenocarcinoma stem cells. Oncol. Lett. *9*, 47–54.

iScience, Volume *23*

Supplemental Information

Human Lung Adenocarcinoma-Derived Organoid Models for Drug Screening

Zhichao Li, Youhui Qian, Wujiao Li, Lisa Liu, Lei Yu, Xia Liu, Guodong Wu, Youyu Wang, Weibin Luo, Fuyuan Fang, Yuchen Liu, Fei Song, Zhiming Cai, Wei Chen, and Weiren Huang

Supplemental Information

Supplemental Figures

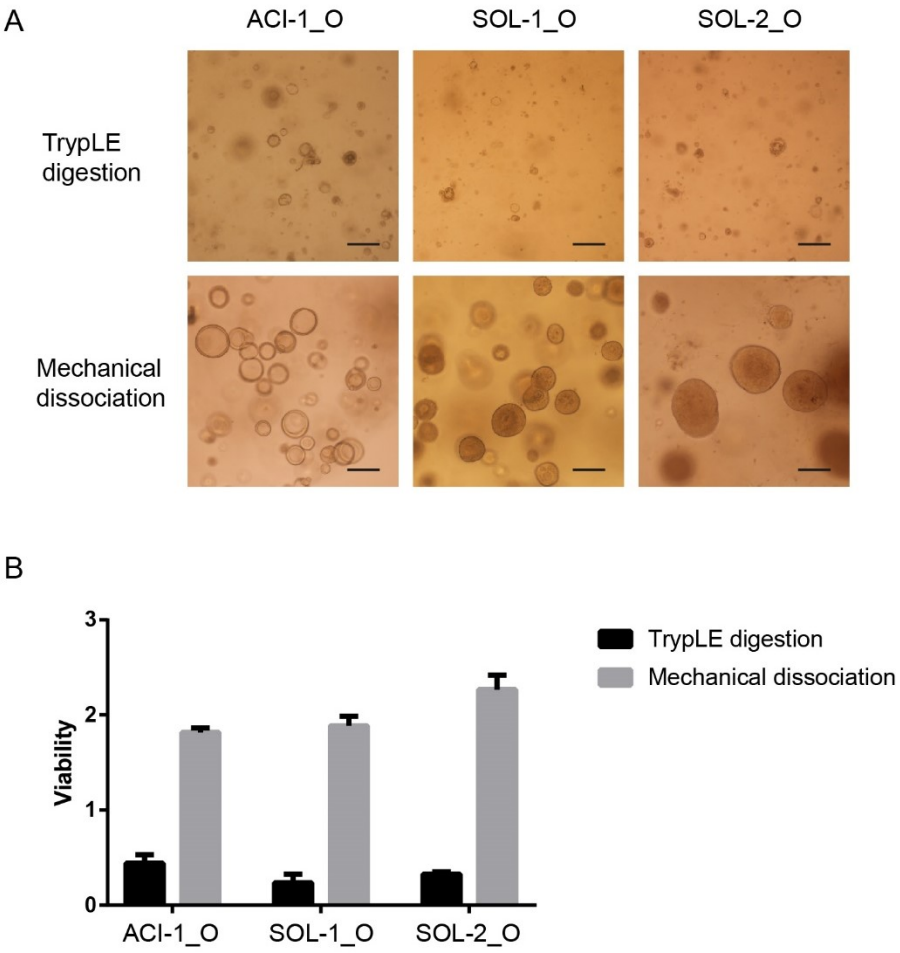

Figure S1. Comparative analysis of dissociation methods for the passage of LADC organoids, Related to Figure 1. (**A**) Representative bright-field images of organoids after passage using the indicated dissociation methods (14 days after passage). Scale bar, 100 μm. (**B**) Quantification of viable cells after passage using the indicated dissociation methods.

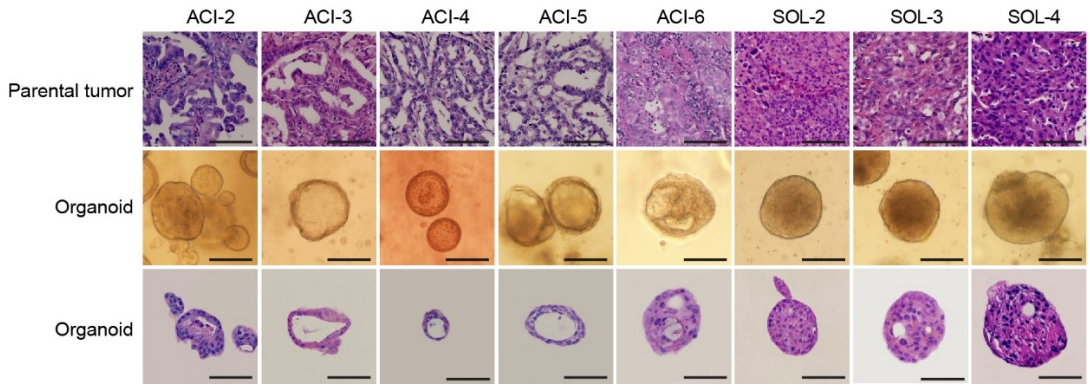

Figure S2. Histological analysis of LADC organoids, Related to Figure 1. H&E staining of LADC organoids and parental tumors, together with the bright-field images of LADC organoids (except for those that are shown in Figure 1C). Scale bar, 100 μm.

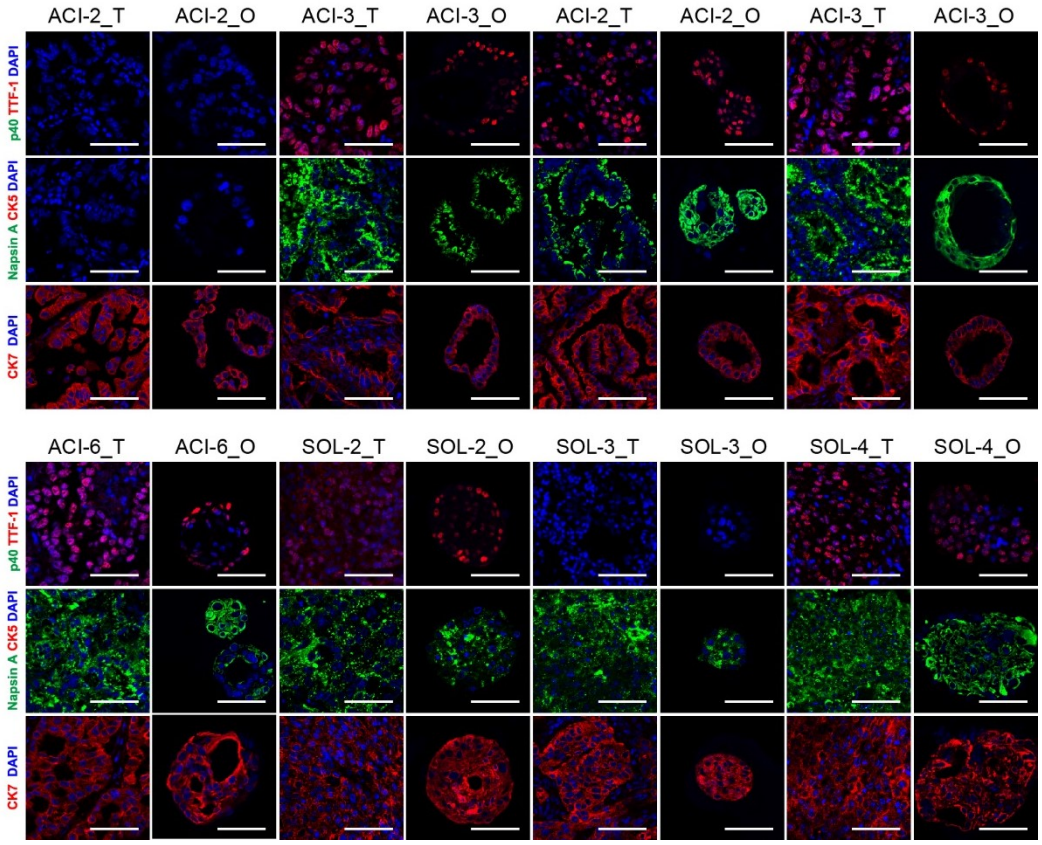

Figure S3. Immunofluorescence images of LADC organoids, Related to Figure 2. Shown above are the representative immunofluorescence images of the LADC organoids (_O) and their corresponding tumor tissues (_T) for p40, TTF-1, Napsin A, CK5, CK7 and DAPI. Scale bar, 100 μm.

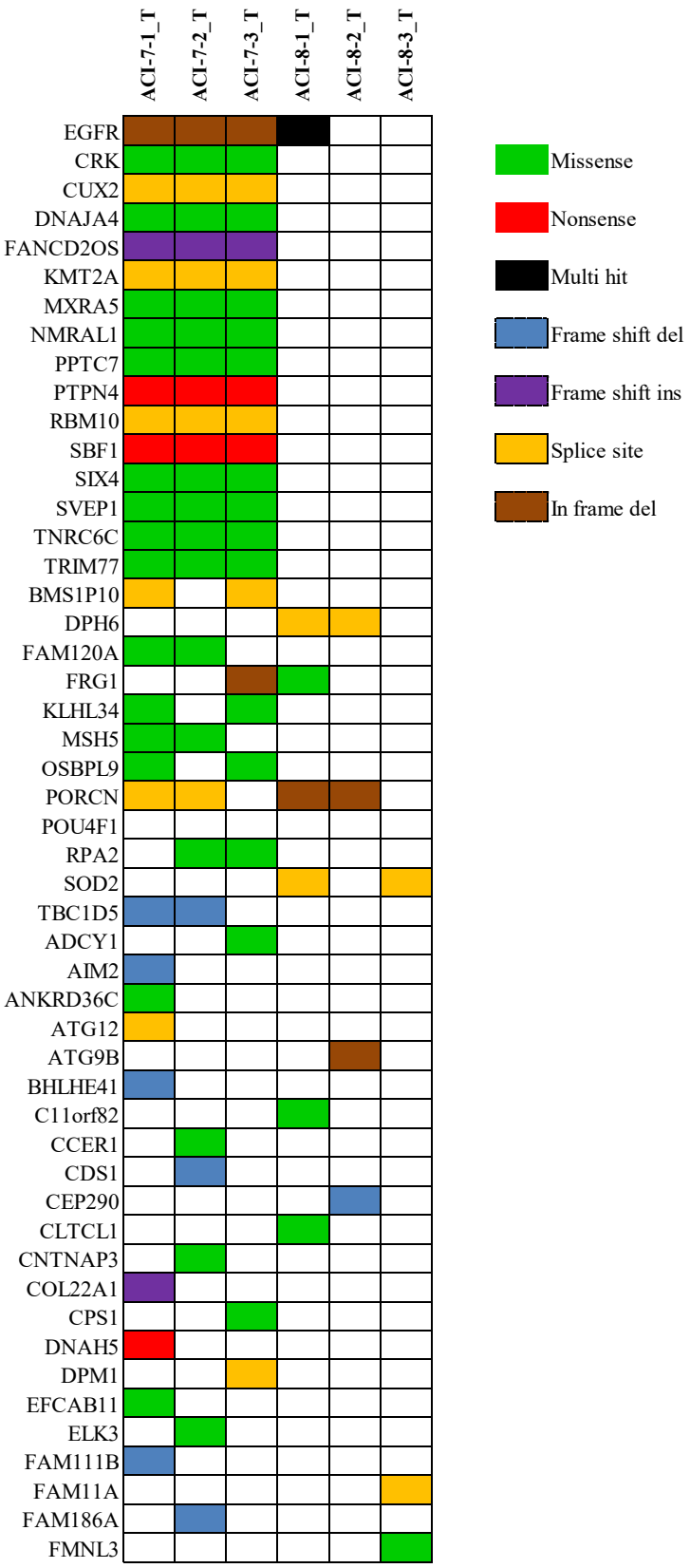

Figure S4. Mutational changes detected by deep targeted sequencing of subregion samples, Related to Figure 3. The type of mutations is indicated in the legend.

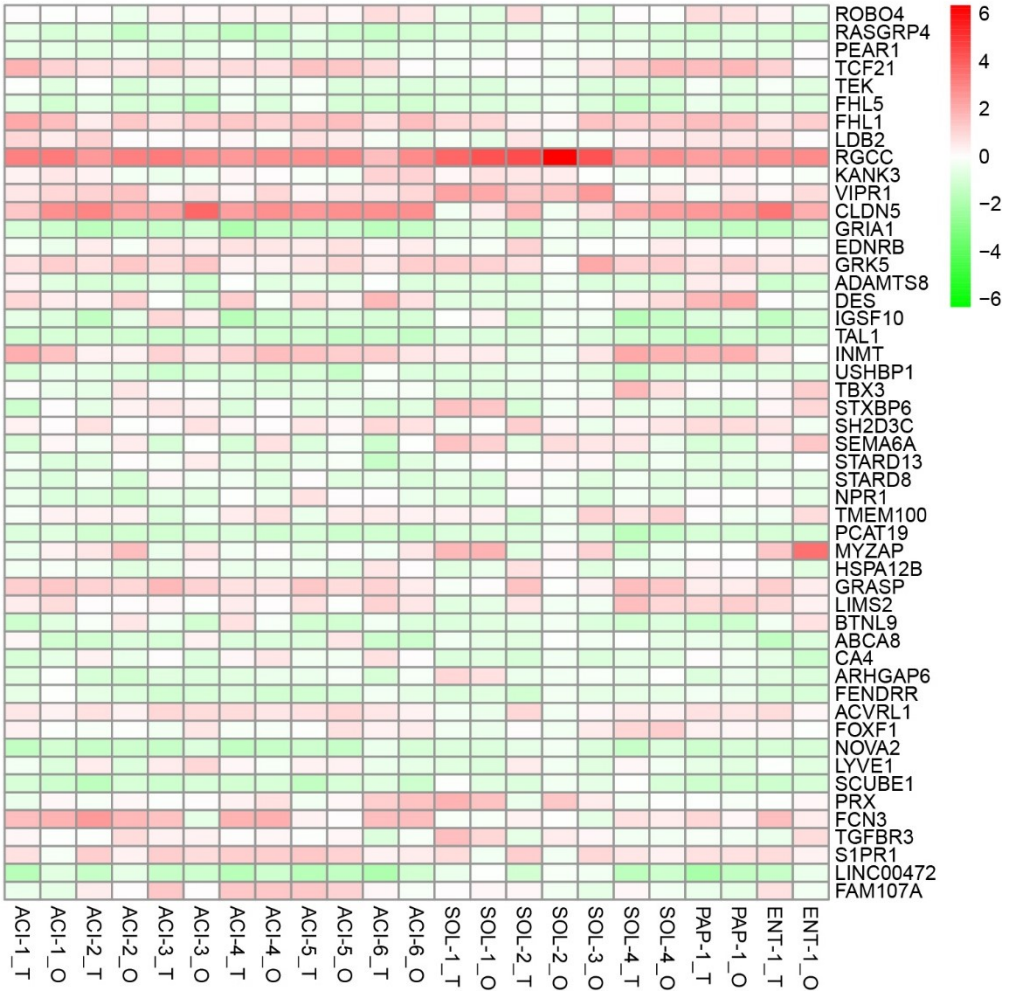

Figure S5. Gene expression heatmap of the top 50 LADC specific genes in LADC organoids (_O) and their parental tumors (_T), Related to Figure 4.

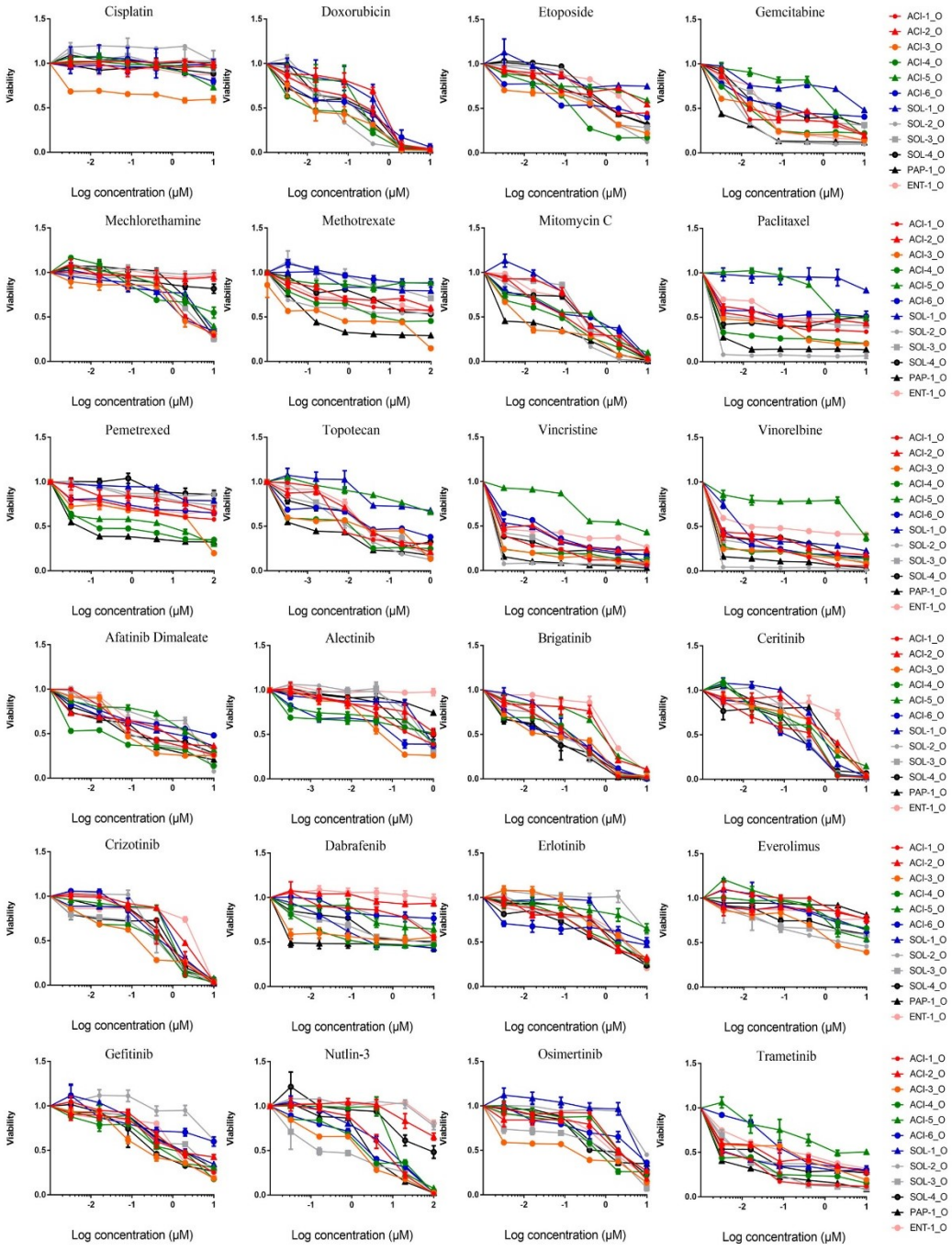

Figure S6. Dose response curves of LADC organoid lines to selected drugs, Related to Figure 6.

Supplemental Tables

Table S1. LADC organoid media recipe, Related to Figure 1.

Reagent Name	Supplier	Catalogue number	Final Concentration in Media
Advanced DMEM/F-12	Thermo Fisher Scientific	12634-010	1x
Antibiotic-Antimycotic (100X)	Thermo Fisher Scientific	15240-062	1x
GlutaMAX™ Supplement	Thermo Fisher Scientific	35050-061	1x
HEPES	Thermo Fisher Scientific	15630-080	10 mM
B-27™ Supplement (50X), serum free	Gibco	17504-044	1x
N-Acetylcysteine	Sigma	A9165	1.25 mM
Nicotinamide	Sigma	N0636	10 mM
SB202190	Sigma	S7076	10 mM
A83-01	Sigma	SML0788	500 nM
Recombinant Human R-Spondin 1 Protein	R&D Systems	4645-RS-250	500 ng/mL
Human Noggin	Peprotech	120-10C-1000	100 ng/mL
Y-27632	Abmole Bioscience	M1817	10 mM
Recombinant Human FGF-10	Peprotech	100-26	20 ng/mL
Recombinant Human KGF (FGF-7)	Peprotech	100-19	25 ng/mL

Table S2. Patients' information, Related to Figure 1.

Line	Diagnosis	Overall tumor stage	Metastasis	Gender	Age	Smoking
ACI-1_O	ACI	II	No	F	68	No
ACI-2_O	ACI	II	No	F	74	No
ACI-3_O	ACI	II	Yes, nodal metastasis	M	77	No
ACI-4_O	ACI	II	Yes, nodal metastasis	F	69	No
ACI-5_O	ACI	I	No	F	66	No
ACI-6_O	ACI	I	No	M	70	Yes
ACI-7	ACI	I	NO	F	66	No
ACI-8	ACI	II	NO	M	55	No
SOL-1_O	SOL	III	No	M	43	No
SOL-2_O	SOL	III	No	M	46	Yes
SOL-3_O	SOL	III	Yes, pleural metastasis	M	49	No
SOL-4_O	SOL	III	No	F	60	No
PAP-1_O	PAP	I	No	F	64	No
ENT-1_O	ENT	II	Yes, nodal metastasis	M	47	Yes

M: male, F: female

Line	Passage number for WES	Passage number for RNA seq	Passage number for HE staining and IF	Passage number for drug screening replicate 1	Passage number for drug screening replicate 2	Passage number for drug screening replicate 3
ACI-1_O	6	6	Early: 6; Late: 11	5	7	10
ACI-2_O	7	7	6	5	8	9
ACI-3_O	7	7	8	5	7	9
ACI-4_O	6	6	7	5	7	9
ACI-5_O	6	6	7	6	7	9
ACI-6_O	7	7	8	6	8	10

SOL-1_O	6	6	Early: 6; Late: 12	6	8	10
SOL-2_O	6	6	6	5	7	9
SOL-3_O	6	6	6	6	8	9
SOL-4_O	6	6	7	6	7	9
PAP-1_O	7	7	Early: 8; Late: 11	6	8	10
ENT-1_O	6	6	Early: 6; Late: 13	6	8	10

Table S3. Antibody information, Related to Figure 2.

Primary antibodies	Antigen	Supplier	Catalogue number	Origin	Dilution
	p40	Maixin Biotech	RAB-0666	rabbit	1/100
	TTF1	Maixin Biotech	MAB-0677	mouse	1/100
	Napsin A	Maixin Biotech	MAB-0704	mouse	1/100
	CK5	Thermo Fisher	RM-2106-S0	rabbit	1/100
	CK7	Thermo Fisher	180234	mouse	1/200
	SFTPC	Thermo Fisher	PA5-71680	rabbit	1/100
Secondary antibodies	Reagent Name	Supplier	Catalogue number	Origin	Dilution
	Donkey anti-Rabbit IgG (H+L) Highly Cross Adsorbed Secondary Antibody, Alexa Fluor 488	Thermo Fisher	A21206	donkey	1/1000
	Goat anti-Mouse IgG (H+L) Cross-Adsorbed Secondary Antibody, Alexa Fluor 555	Thermo Fisher	A21422	goat	1/1000

Table S6. List of drugs screened, Related to Figure 6.

Drug Name	Supplier	Catalogue number	Target	Max Concentration (μM)
Afatinib	Selleck Chemicals	S7810	EGFR/HER2	10 μM
Alectinib	Selleck Chemicals	S2762	ALK	1 μM
Brigatinib	Selleck Chemicals	S8229	ALK	10 μM
Ceritinib	Selleck Chemicals	S7083	ALK	10 μM
Cisplatin	Sigma	1134357	DNA crosslinker	10 μM
Crizotinib	Selleck Chemicals	S1068	ALK, c-Met	10 μM
Dabrafenib	Selleck Chemicals	S2807	BRAF	10 μM
Doxorubicin	Sigma	PHR1789	DNA replication	10 μM
Erlotinib	Selleck Chemicals	S1023	EGFR	10 μM
Etoposide	Selleck Chemicals	S1225	Topoisomerase II	10 μM
Everolimus	Sigma	E068 CERILLIANT	mTOR	10 μM
Gefitinib	Selleck Chemicals	S1025	EGFR	10 μM
Gemcitabine	Sigma	1288463	DNA replication	10 μM
Mechlorethamine	Selleck Chemicals	S4252	DNA crosslinker	10 μM
Methotrexate	Sigma	M9929	DHFR	100 μM
Mitomycin C	Selleck Chemicals	S8146	DNA crosslinker	10 μM
Nutlin-3a	Selleck Chemicals	S1061	MDM2	100 μM
Osimertinib	Selleck Chemicals	S7297	EGFR	10 μM
Paclitaxel	Selleck Chemicals	S1150	Tubulin	10 μM
Pemetrexed	Selleck Chemicals	S7785	TS, DHFR, GARFT	100 μM

Topotecan	Selleck Chemicals	S1231	Topoisomerase I	1 μM
Tramatenib	Selleck Chemicals	S2673	MEK1/2	10 μM
Vincristine	Selleck Chemicals	S1241	Tubulin	10 μM
Vinorelbine	Selleck Chemicals	S4269	Tubulin	10 μM

Transparent Methods

Tumor Specimen Collection

Lung adenocarcinoma (LADC) samples (1-4 cm^3) were obtained from the Second People's Hospital of Shenzhen and were transported directly to the laboratory after the surgery was performed. All patients provided informed consent. The study was approved by the Ethics Committee of the First Affiliated Hospital of Shenzhen University. Please see Table S2 for the clinical details of these samples.

Organoid Culture

Tumor samples were washed twice with cold PBS before minced into smaller pieces using scissors. A small piece was fixed in formalin for histopathological analysis and immunofluorescence. Half of the minced samples were frozen and stored in -80ºC for DNA and RNA isolation, while the other half was used for the isolation of cancer cells. The minced tissue was incubated with collagenase II (5 mg/mL) with ROCK inhibitor Y-27632 dihydrochloride (10 μM) for 1 h at 37 °C. Digested tissues were spun down at 200 g for 5 min, washed once with AdDMEM/F12, and spun down again. The tissues were suspended in 5 mL of TrypLE Express with Y-27632 dihydrochloride (10 μM) for ~10 min at 37 °C. Trypsinization was stopped by the addition of 10 mL of AdDMEM/F12 supplemented with 1% penicillin/streptomycin, 1% Glutamax, 1% HEPES (Gibco), and 20% FBS. The dissociated cells were centrifuged at 200 g for 5 minutes and washed once with AdDMEM/F12 before being filtered through a 70-μM

cell strainer to remove large undigested clusters. The cells were centrifuged at 200 g for 5 minutes and resuspended with cold Matrigel. Six drops of 50-µL Matrigel-cell mixture (~20,000 cells/drop) were plated into one well of a 6-well plate. The drops were solidified for 2 minutes right side up and for another 8 minutes upside down at 37°C and 5% CO_2. After the drops solidified, 2.5 mL of LADC organoid medium was added to each well. See Table S1 for the composition of the LADC organoid medium. The medium was replaced every 3 days and fresh medium was made weekly.

For passaging, Matrigel drops were scraped from the plate and centrifuged at 200 g for 3 minutes. The supernatant was discarded and the Matrigel was digested with TrypLE Express with Y-27632 dihydrochloride (10 µM) for ~5 min at 37 °C. The trypsinization was stopped by the addition of 10 mL of AdDMEM/F12 supplemented with 1% penicillin/streptomycin, 1% Glutamax, 1% HEPES, and 20% FBS. Organoids were centrifuged at 200 g for 5 min, washed once with AdDMEM/F12, and centrifuged again. Organoids (2-3 weeks after starting the culture) were dissociated into smaller clusters through trituration with 10 mL Stripette Serological Pipets. Organoids were passaged at a 1:2-1:3 ratio every 2-3 weeks.

To cryo-preserve organoids, organoids were dissociated from the Matrigel, and then frozen in recovery-cell-culture freezing medium (GIBCO) with Y-27632 dihydrochloride (10 µM).

Histology and Immunostaining

Tissues were washed in PBS and fixed and stored in 10% formalin before embedding and sectioning. Organoids were harvested and dissociated from the Matrigel, and fixed in 10% formalin.

Hematoxylin-eosin (H&E) staining and immunostaining were performed on 4 µm paraffin sections of cultured organoids and parental tumors. For H&E staining, paraffin sections were deparaffinized in xylene and rehydrated through a graded-ethanol series.

For immunofluorescence experiments, paraffin slides were subjected to antigen retrieval using EDTA solution (pH 8.0) after being deparaffinized and rehydrated. Sections were blocked in BSA blocking buffer (5% BSA in PBS) for 1 h at 37 °C and incubated with diluted primary antibodies (listed in Table S3) overnight at 4 °C. Slides were then washed with PBS and incubated with diluted secondary antibodies (listed in Table S3) for 1 h at room temperature. Nuclei were counterstained with DAPI. Immunofluorescence was imaged using a ZEISS confocal microscope.

Whole-Exome Sequencing and Analysis

The genomic DNA and RNA were isolated from primary tissue, blood, and organoids using the AllPrep DNA/RNA Mini Kit. Whole-Exome Sequencing (WES) libraries were generated using Agilent SureSelect Human All Exon V6 kit (Agilent Technologies, CA, USA) following manufacturer's recommendations and index codes were added to each sample. The WES libraries were sequenced with paired-end (2 X 150 bp) runs using Illumina X ten. The blood samples were sequenced to depths of 100 X (~12 Gb per sample) and tumor and organoids samples were ~200X (~24 Gb per sample). The sequencing data were filtered by adaptor and low quality reads by Fastp (v 0.12.6) (Chen et al., 2018). SNV were detected by GATK(v3.6) (McKenna et al., 2010). According to best practices guidelines, sequence reads were mapped against the human reference genome (UCSC hg19) using Burrows-Wheeler Alignment with maximal exact matches (BWA-MEM) v0.7.12 (Li and Durbin, 2009) followed by marked duplicates, merging of lanes, and realignment of INDELs. Base recalibration was not performed. Somatic SNVs and INDELs were determined by providing the reference (Blood) and tumor or organoid sequencing data to Mutect2 (options: -mbq 15 -allowPotentiallyMisencodedQuals) and Strelka2 (Kim et al., 2018) separately. Somatic SNVs with VAF<0.05 and supported by less than 3 reads were filtered out. CNAs were detected by Control-FREEC (v11.5) (Boeva et al., 2012) with BAM files. Mutation effect predictions and annotations were performed by Annovar (v) (Wang et al., 2010), COSMIC and dbSNP (Sherry et al., 2001).

RNA sequencing and analysis

RNA extraction was performed as described above. Sequencing libraries were generated using NEBNext® UltraTM RNA Library Prep Kit for Illumina® (NEB, USA) following the manufacturer's recommendations, and index codes were added to attribute sequences to each sample. The RNA libraries were sequenced with PE 150 bp using Illumina X ten. Low quality and adaptor polluted reads were removed. Then sequence reads were aligned to the reference genome (UCSC hg19) using STAR(v2.4.0j) (Dobin et al., 2013). Gene expression analysis was performed by RSEM (Li and Dewey, 2011), and differentially expressed genes were identified by EdgeR (Robinson et al., 2010).

We downloaded Level 3 RNA-seq LADC data from the TCGA Data Portal, and a total of 541 LADC samples' count data were used for analysis as provided. We normalized the expression data of the organoids and TCGA tumors together using ComBat (Leek et al., 2012), followed by normalization for sequencing depth and log10-transformation. Organoids and TCGA samples were clustered using the hclust function in R.

Principal components analysis (PCA) for normal lung tissue-derived organoids and LADC organoids were calculated by plotPCA function using the normalized EdgeR counts, the first two (PC1, PC2) were plotted. KEGG pathway enrichment of differentially expressed were performed by clusterProfiler.

We calculated differentially expressed genes between normal lung organoids and LADC organoids, then 30 upregulated genes and 30 downregulated genes in LADC organoids with the lowest *p*-value were listed. The survival analysis was performed using GEPIA server.

Organoid Drug Screening

To plate organoids for the drug screening, organoids were collected 5 days after passaging and filtered through a 100-μm cell strainer to remove large organoids. Collected organoids were resuspend in 2% Matrigel growth medium (20,000 organoids/mL) and dispensed into ultra-low attachment 96-well plates (100 μL/well) in triplicates. A 6-point 5-fold dilution series of 24 drugs (Listed in Table S6) were dispensed 24 h after plating. The maximal concentration of each drugs can be found in Table S6. Cell viability was assayed after 6 days of drug incubation using Cell Titer-Glo 3D (Promega) according to the manufacturer's instructions. Screens were performed in technical duplicates and biological triplicates.

Data analyses were performed using GraphPad Prism 7, the values of the IC_{50} and AUC were calculated by using nonlinear regression (curve fit) on the equation log (inhibitor) versus normalized response (variable slope).

Statistical Analysis

Statistical analyses were performed using GraphPad Prism 7. All summary data are presented as mean ± SEM, unless otherwise specified.

References

Boeva, V., Popova, T., Bleakley, K., Chiche, P., Cappo, J., Schleiermacher, G., Janoueix-Lerosey, I., Delattre, O., and Barillot, E. (2012). Control-FREEC: a tool for assessing copy number and allelic content using next-generation sequencing data. Bioinformatics (Oxford, England) 28, 423-425.

Chen, S., Zhou, Y., Chen, Y., and Gu, J. (2018). fastp: an ultra-fast all-in-one FASTQ preprocessor. Bioinformatics (Oxford, England) 34, i884-i890.

Dobin, A., Davis, C.A., Schlesinger, F., Drenkow, J., Zaleski, C., Jha, S., Batut, P., Chaisson, M., and Gingeras, T.R. (2013). STAR: ultrafast universal RNA-seq aligner. Bioinformatics (Oxford, England) 29, 15-21.

Kim, S., Scheffler, K., Halpern, A.L., Bekritsky, M.A., Noh, E., Kallberg, M., Chen, X., Kim, Y., Beyter, D., Krusche, P., et al. (2018). Strelka2: fast and accurate calling of germline and somatic variants. Nature methods 15, 591-594.

Leek, J.T., Johnson, W.E., Parker, H.S., Jaffe, A.E., and Storey, J.D. (2012). The sva package for removing batch effects and other unwanted variation in high-throughput experiments. Bioinformatics (Oxford, England) 28, 882-883.

Li, B., and Dewey, C.N. (2011). RSEM: accurate transcript quantification from RNA-Seq data with or without a reference genome. BMC bioinformatics 12, 323.

Li, H., and Durbin, R. (2009). Fast and accurate short read alignment with Burrows-Wheeler transform. Bioinformatics (Oxford, England) 25, 1754-1760.

McKenna, A., Hanna, M., Banks, E., Sivachenko, A., Cibulskis, K., Kernytsky, A., Garimella, K., Altshuler, D., Gabriel, S., Daly, M., et al. (2010). The Genome Analysis Toolkit: a MapReduce framework for analyzing next-generation DNA sequencing data. Genome research 20, 1297-1303.

Robinson, M.D., McCarthy, D.J., and Smyth, G.K. (2010). edgeR: a Bioconductor package for differential expression analysis of digital gene expression data. Bioinformatics (Oxford, England) 26, 139-140.

Sherry, S.T., Ward, M.H., Kholodov, M., Baker, J., Phan, L., Smigielski, E.M., and Sirotkin, K. (2001). dbSNP: the NCBI database of genetic variation. Nucleic acids research 29, 308-311.

Wang, K., Li, M., and Hakonarson, H. (2010). ANNOVAR: functional annotation of genetic variants from high-throughput sequencing data. Nucleic acids research 38, e164.